Large-Deformation Image Registration using Fluid Landmarks

G.E. Christensen[1], P. Yin[1], M.W. Vannier[2], K.S.C. Chao[3], J.F. Dempsey[3], and J.F. Williamson[3]
[1]Department of Electrical and Computer Engineering
The University of Iowa, Iowa City, IA, 52242, USA
[2]Department of Radiology
The University of Iowa, Iowa City, IA, 52242, USA
[3]Mallinckrodt Institute of Radiology
Washington University, St. Louis, MO, 36110, USA

Abstract

For each patient receiving definitive treatment for cervix cancer, several CT/MR imaging studies need to be registered in order to specify the total physical or biological dose to each fixed tissue voxel in an organ system. This turns out to be a difficult problem due to large localized deformations and displacements of bladder, rectum, vagina, uterus and paracervical tissues due to tumor regression, bladder and rectal filling variations, and especially insertion of the applicator itself. This paper explores the utility of using the fluid landmark image registration method to register images before and after insertion of the brachytherapy applicator in order to track radiation dose from one treatment to the next.

1 Introduction

Cervical cancer is the second most common malignancy found in women after breast cancer and affects approximately 500,000 women annually worldwide. Every year in the United States, approximately 15,000 women are diagnosed with cervical cancer and 5,000 women die of the disease. One common treatment for cervical cancer is intracavitary brachytherapy radiation therapy in which a high dose of radiation is delivered to the site of the tumor by inserting an applicator into the vagina/uteral canal. Most brachytherapy treatment plans are made from 2D bilateral x-rays and ignore the soft-tissue deformation of the pelvic anatomy from one examination to the next due to insertion of brachytherapy applicators, tumor regression, and soft-tissue movement. Imaging the pelvis with CT before and after each applicator insertion, it is possible to visualize the 3D deformation of the soft-tissue structures. We are studying methods for registering these image volumes together in order to specify the total physical or biological dose to each fixed tissue voxel in an organ system. Common image registration techniques based on thin-plate splines and linear-elastic models [10, 1, 2, 8] have a small deformation assumption and can not be used due to the large localized deformations associated with this problem. This paper explores the utility of using the fluid landmark image registration method [7, 9, 6] for this problem. The fluid model [4] has no small deformation assumption and is therefore able to track large localized nonlinear deformations.

The images to be registered are 3D CT volumes of the same patient imaged at different times before and during intracavitary brachytherapy radiation therapy. We seek to find an invertible transformation that maps corresponding voxels in an image with the applicator to their corresponding locations in a target image without the applicator. These transformations must accommodate the large localized soft-tissue deformation of the pelvic anatomy from one examination to the next due to insertion of brachytherapy applicators, tumor regression, and soft-tissue movement. The transformation found from the image registration provides a dense correspondence map between images that is used to track the cumulative radiation dose that each volume element of tissue receives over the course of treatment. We have shown [5] that a volumetric fluid image registration method [4] is able to accommodate the large localized soft-tissue deformation of the pelvic anatomy. In this approach, the 3D fluid transformation from one image to another was found by matching the 3D CT data and manually generated segmentations of the vagina, uterus, bladder, and rectum.

A drawback of the volumetric fluid image registration method for registering segmentations is that it is computationally inefficient. This inefficiency is due to the fact that the volumetric algorithm estimates a volumetric transformation at each iteration. However, the segmentations only add information at their surfaces. Therefore, it is more efficient to only estimate the transformation at the surfaces of the

segmentations at each iteration and then extend the transformation to the full volume after the surfaces are matched. It is for this reason that we are investigating using the fluid landmark image registration algorithm.

In this current work we restrict our problem to that of matching 2D images and therefore the surface matching problem becomes a contour matching problem. A contour can be discretized into an ordered set of points that when connected by straight lines forms the original curve. We discretized each corresponding curve in the template image and the target image into an equal number of points. The correspondence between two curves can then be reduced to matching the corresponding discretized node points of each contour. The fluid landmark image registration algorithm is then used to deform one image into the other by matching the corresponding node points of the discretized contours.

Matching contours is computationally more efficient than matching segmented subvolumes because there are fewer parameters to estimate. However, defining exact landmark correspondences between structures is not always possible on smooth structures and therefore matching segmented subvolumes—which avoids this problem—should be used. In the future, we plan to combine the landmark and intensity-based fluid registrations algorithms as we have done for linear-elastic image registration [3].

2. Fluid landmark registration

We follow the fluid landmark image registration approach of Joshi et al. [7, 9, 6]. In the next three sections, we will discuss the general formulation of the fluid landmark problem, how this problem can be solved efficiently by reducing the dimensionality of the problem, and how this solution is converted back to the full dimensional solution.

2.1. The landmark matching problem

The landmark mapping problem is based on a finite number of N landmark points, where template landmark set $I_0 \doteq \{y_n\}_{n=1}^N \subset \Omega$ and target landmark set $I_1 \doteq \{x_n\}_{n=1}^N \subset \Omega$, $\Omega = R^3$ for three dimensional problem. It is assumed that the manual identification of landmarks is a random process with some mean and variance. The spatial variance of placing the landmarks corresponds to the accuracy with which landmarks can be repeatably identified. For example, placing a landmark at the intersection of two lines would have a low variance while placing a landmark at a high curvature point of an anatomic structure would have a high variance. This spatial placement variance may be isotropic or anisotropic. An example of an isotropic landmark placement error would be identifying the center of a spherical fiducial marker. An anisotropic placement error occurs when placing a landmark on a 3D contour; the landmark is easy to place in the two orthogonal directions to the contour, but is more variable alone the contour. The spatial landmark identification error covariance between the x, y, and z coordinates for each landmark is denoted by $\sum_n$, $n = 1, \cdots, N$.

This landmark matching algorithm works directly on the Lagrangian trajectory $\phi(x,t)$ of the landmarks. $\phi(x,t)$ is defined as the position of a landmark at time t which was at x at time 0. The trajectories can be parameterized via rate of change associated with their velocity fields

$$\phi(x,T) = x + \int_0^T v(\phi(x,t),t)dt \tag{1}$$

Diffeomorphic transformations are constructed by forcing the velocity fields to be associated with quadratic energetics on $\Omega \times [0,T] \in R^4$ defined via the form $E(v) = \int_{\Omega\times[0,T]} \|Lv(x,t)\|^2 dxdt$, where L is a constant coefficient, 3×3 matrix differential operator.

Define $3N \times 1$ vector for time paths of the N landmarks

$$\Phi(t) = [\phi(y_1,t), \phi(y_1,t), \cdots, \phi(y_N,t)]^t \tag{2}$$

To match end point conditions of the landmarks, landmark distance function $D(\Phi)$ of following form is used

$$D(\Phi(T)) \doteq \sum_{n=1}^N [x_n - \phi(y_n,T)]^t \sum_n^{-1} [x_n - \phi(y_n,T)] \tag{3}$$

Therefore, the optimal landmark matching problem can be stated as

$$\hat{v}(x,t) = argmin_{v(x,t)} \int_0^T \int_\Omega \|Lv(x,t)\|^2 dxdt + D(\Phi(T)) \tag{4}$$

and

$$\hat{\phi}(x,T) = x + \int_0^T \hat{v}(\hat{\phi}(x,t))dt \tag{5}$$

2.2. Solving the optimum time paths of the landmarks

It is proven by Joshi in [7] that by reformulating the minimization problem in Eq.(4), the optimal path of N landmarks $\hat{\Phi}(t)$ would satisfy following minimization problem

$$\begin{aligned}\hat{\Phi}(t) = argmin_{\Phi(t)} &\int_0^T \dot{\Phi}(t) K^{-1}(\Phi(t)) \dot{\Phi}(t) dt \\ &+ \sum_{n=1}^N [x_n - \phi(y_n,T)]^t \sum_n^{-1} [x_n - \phi(y_n,T)]\end{aligned} \tag{6}$$

subject to $\Phi(0) = [y_1, y_2, \cdots, y_N]^t$.

$K(\Phi(t))$ in Eq.(6) is a $3N \times 3N$ matrix. The $ij - 3 \times 3$ block of $K(\Phi(t))$ is

$$(K(\Phi(t)))_{ij} = k(\phi(y_i, t), \phi(y_j, t)) \tag{7}$$

$k(x, x^{'})$ is the 3×3 covariance matrix function corresponding to the Green's function squared of the differential operator L in Eq.(4). In this implementation, L is set to a diagonal 3×3 Laplacian operator differentiating in space. That is, $L = diag(-\nabla^2 + c)$ and

$$k(x, x^{'}) = 2\sqrt{c}(2\pi)^{5/2} e^{\frac{-1}{\sqrt{c}}\|x - x^{'}\|} I \tag{8}$$

where I is the 3×3 identity matrix. The power of working with $\Phi(t)$ is that the optimization has been reduced from velocity fields on $\Omega \times [0, T]$ to N time path fields $\Phi(t)$ on $[0, T]$.

To solve the minimization problem in Eq.(6), the problem is reduced to finite dimensional by defining the transformation on finite grid of fixed size time intervals. Divide the time $[0, T]$ into M intervals $\{t_i = \frac{Ti}{M}\}_{i=0}^{M}$, and define $\Phi_i = \Phi(t_i)$. Assume the velocities are piecewise constant within quantized time intervals, so that for $t \in [t_i, t_{i+1})$,

$$\dot{\Phi}(t) = \frac{\Phi_{i+1} - \Phi_i}{\frac{T}{M}} \tag{9}$$

Rewrite Eq.(6) as

$$\hat{\Phi}(t) = argmin_{\Phi(t)}(P(\Phi(t)) + D(\Phi(t))) \tag{10}$$

and

$$P(\Phi(t)) = \int_0^T \dot{\Phi}(t) K^{-1}(\Phi(t)) \dot{\Phi}(t) dt \tag{11}$$

$$D(\Phi(t)) = \sum_{n=1}^{N} [x_n - \phi(y_n, T)]^t \Sigma_n^{-1} [x_n - \phi(y_n, T)] \tag{12}$$

Also make the assumption that $K(\Phi(t))$ does not change over $t \in [t_i, t_{i+1})$, then

$$P(\Phi(t)) = \frac{T}{M} \sum_{i=0}^{M-1} \frac{(\Phi_{i+1} - \Phi_i)^t}{\frac{T}{M}} K^{-1}(\Phi_i) \frac{(\Phi_{i+1} - \Phi_i)}{\frac{T}{M}} \tag{13}$$

Eq.(6) can be solved by iterative gradient descent,

$$\Phi_i^{k+1} = \Phi_i^k - \epsilon(\frac{\partial P(\Phi(t))}{\partial \Phi_i} + \frac{\partial D(\Phi(t))}{\partial \Phi_i}) \tag{14}$$

where Φ_i^k is the estimate of Φ_i at iteration k, and ϵ is step size. Also, we have

$$\begin{aligned} &\frac{\partial P(\Phi(t))}{\partial \Phi_i} \\ &= \frac{T}{M}(\frac{(\Phi_{i+1} - \Phi_i)^t}{\frac{T}{M}} K^{-1}(\Phi_i) \frac{dK(\Phi_i)}{d\Phi_i} K^{-1}(\Phi_i) \frac{(\Phi_{i+1} - \Phi_i)}{\frac{T}{M}} \\ &\quad - 2K^{-1}(\Phi_i) \frac{(\Phi_{i+1} - \Phi_i)}{\frac{T^2}{M^2}} + 2K^{-1}(\Phi_{i-1}) \frac{(\Phi_i - \Phi_{i-1})}{\frac{T^2}{M^2}}) \end{aligned} \tag{15}$$

Define target landmark set $X = [x_1, x_2, \cdots, x_N]$,

$$\frac{\partial D(\Phi(t))}{\partial \Phi_i} = \begin{cases} 2\Sigma_i^{-1}[\Phi(T) - X] & i = M \\ 0 & i < M \end{cases} \tag{16}$$

2.3. Finding the transformation for the full image space

The optimum landmark time paths estimated from last section can be used to calculate transformation associated with the whole image space. Assume ITR is the total number of iterations and final iteration $\hat{\phi} = \phi^{(ITR)}$, then for $t \in [t_{i-1}, t_i)$,

$$\dot{\hat{\phi}}(y_n, t) = \frac{\hat{\phi}(y_n, t_i) - \hat{\phi}(y_n, t_{i-1})}{\frac{T}{M}} \tag{17}$$

Velocity vectors associated the whole image space $x \in \Omega$ can be obtained by following equation,

$$\hat{v}(x, t) = \sum_{n=1}^{N} k(\hat{\phi}(y_n, t), x) \sum_{j=1}^{N} (K^{-1}(\hat{\Phi}(t)))_{nj} \dot{\hat{\phi}}(y_j, t) \tag{18}$$

and final trajectories associated the whole image space can be estimated by

$$\hat{\phi}(x, T) = \int_0^T \hat{v}(\hat{\phi}(x, t), t) dt + x \tag{19}$$

3. Results

In this paper we use contours to define the correspondences between two images (see Fig. 1) instead of the segmented subvolumes as in [5]. The contours in each image are discretized by defining a set of N, ordered landmarks sampled along the contours. The correspondence between the landmarks on the contours defines the correspondence between the contours. The fluid landmark algorithm is used to register the two images by matching the images at these landmarks. The landmarks in the template image were selected at uniform spacing around the contour. The landmarks in the target image were found by identifying the

landmark locations in the target contour that corresponded to the five landmarks in the template with the highest curvature. The rest of the target landmarks were uniformly spaced between these five identified points.

Figure 1 shows a experiment where the landmarks are selected to be along the contour of uterus/vagina to track the shape change of the uterus/vagina during the radiation treatment. The results shown in Fig. 1 suggests that this landmark registration algorithm can correct for large shape deformation of the uterus/vagina. Notice that the transformation is local to the area of the landmarks, and the bony anatomy does not move much after the registration. The transformations are constrained to diffeomorphic, and when the same transformation is applied to square grid, the deformed grid is smooth and never cross over.

4. Discussion

The result shown in Fig. 1 is based on the assumption that there is point to point correspondence between the template and target landmarks. However, defining exact landmark correspondences between structures is not always possible on smooth structures. Fig. 2 shows an example when there is poor correspondence of the landmark points. In this experiment, the same template and target images were used as in the first experiment. However, the landmarks in both the template and the target contours were selected to be uniformly spaced around the contour. The problem in this case was that the template landmark points located at points of high curvature did not correspond to the points of high curvature on the target contour.

Therefore, the implementation of the landmark registration algorithm would be improved if there was a better approach for selecting the landmark points. This problem can also be avoided by matching segmented subvolumes. Therefore, in the future, we plan to combine the landmark and intensity-based fluid registrations algorithms as we have done for linear-elastic image registration [3].

5 Summary

We have shown that the fluid landmark image registration technique is able to accommodate the large localized nonlinear transformations commonly found when registering CT image volumes of before and after insertion of brachytherapy applicators. The major limitation of the current method is the need to accurately identify corresponding landmarks in the template and target image volumes. In future work, we will seek to automatically identify corresponding landmarks and extend this work to 3D.

6 Acknowledgments

This work was supported in part by NIH grants R01-NS35368 and R01-CA75371 and the Whitaker Foundation. We would like to that Sarang C. Joshi for his helpful comments regarding the implementation of the fluid landmark algorithm.

References

[1] Y. Amit, U. Grenander, and M. Piccioni. Structural image restoration through deformable templates. *J. American Statistical Association*, 86(414):376–387, June 1991.

[2] F. Bookstein. *Morphometric Tools for Landmark Data*. Cambridge University Press, New York, 1991.

[3] G. Christensen, S. Joshi, and M. Miller. Volume geometric transformations for mapping anatomy. *IEEE Trans. on Med. Imaging*, 16(6):864–877, December 1997.

[4] G. Christensen, R. Rabbitt, and M. Miller. Deformable templates using large deformation kinematics. *IEEE Transactions on Image Processing*, 5(10):1435–1447, Oct 1996.

[5] G. Christensen, J. Williamson, K. Chao, M. Miller, F. So, and M. Vannier. Deformable anatomical templates for brachytherapy treatment planning in radiotherapy of cervical cancer. In R. Melter, A. Wu, and L. Latecki, editors, *Vision Geometry VI*, Proceedings of SPIE Vol. 3168, pages 147–154, 1997.

[6] U. Grenander and M. I. Miller. Computational anatomy: An emerging discipline. *Quarterly of Applied Mathematics*, LVI(4):617–694, December 1998.

[7] S. Joshi. *Large deformation diffumorphisms and gaussian random fields for statistical characterization of brain submanifolds*. D.Sc. Dissertation, Department of Electrical Engineering, Sever Institute of Technology, Washington University, St. Louis, MO. 63130, Dec 1997.

[8] M. Miller, G. Christensen, Y. Amit, and U. Grenander. Mathematical textbook of deformable neuroanatomies. *Proceedings of the National Academy of Sciences*, 90(24):11944–48, Dec. 1993.

[9] M. Miller, S. Joshi, and G. Christensen. Large deformation fluid diffeomorphisms for landmark and image matching. In A. Toga, editor, *Brain Warping*, pages 115–132. Academic Press, San Diego, 1999.

[10] G. Wahba. *Spline Models for Observational Data*. Society for Industrial and Applied Mathematics, Philadelphia, 1990.

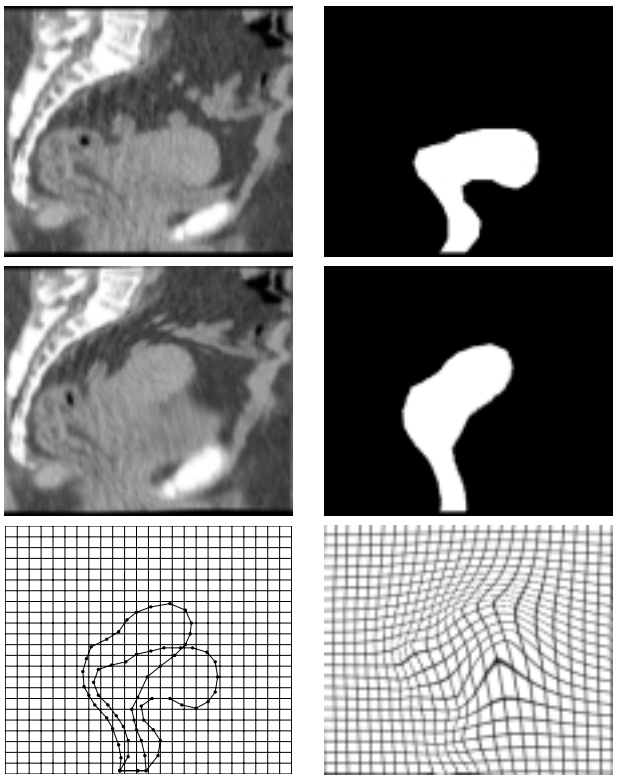

Figure 1. CT and uterus/vagina segmentation of the midsagittal slice from a 3D data set before (top row) and after (middle row) fluid landmark transformation. The bottom-left panel shows the landmarks used to transform the original data set and the bottom-right panel shows the transform applied to a square grid.

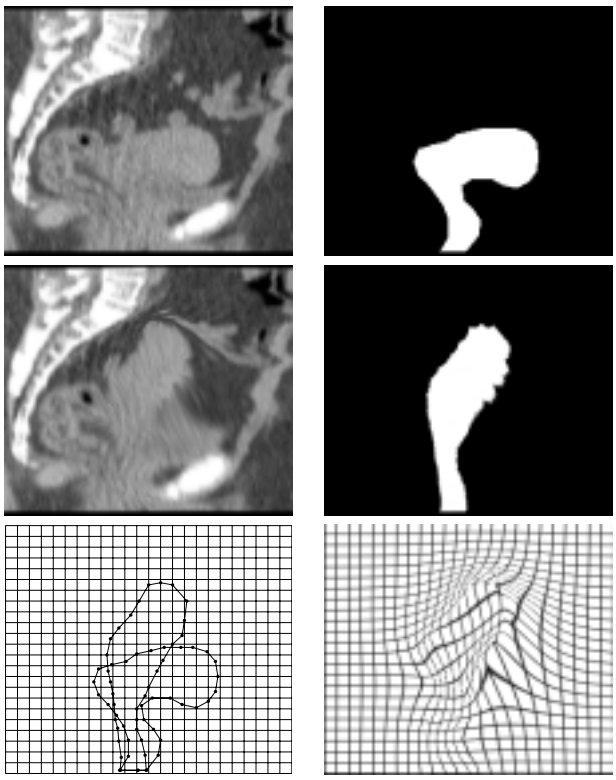

Figure 2. Effect of poor landmark correspondence: CT and uterus/vagina segmentation of the midsagittal slice from a 3D data set before (top row) and after (middle row) fluid landmark transformation. The bottom-left panel shows the landmarks used to transform the original data set and the bottom-right panel shows the transform applied to a square grid.